2-1-2019

Dynamic light scattering optical coherence tomography to probe motion of subcellular scatterers.

Nico J J Arezza

Marjan Razani

Michael C Kolios

Journal of Biomedical Optics

BiomedicalOptics.SPIEDigitalLibrary.org

Dynamic light scattering optical coherence tomography to probe motion of subcellular scatterers

Nico J. J. Arezza
Marjan Razani
Michael C. Kolios

SPIE.

Nico J. J. Arezza, Marjan Razani, Michael C. Kolios, "Dynamic light scattering optical coherence tomography to probe motion of subcellular scatterers," *J. Biomed. Opt.* **24**(2), 025002 (2019), doi: 10.1117/1.JBO.24.2.025002.

Journal of Biomedical Optics 24(2), 025002 (February 2019)

Dynamic light scattering optical coherence tomography to probe motion of subcellular scatterers

Nico J. J. Arezza,[a,b] Marjan Razani,[a,b] and Michael C. Kolios[a,b,*]
[a]Ryerson University, Department of Physics, Faculty of Science, Toronto, Canada
[b]Institute for Biomedical Engineering, Science and Technology, Li Ka Shing Knowledge Institute, St. Michael's Hospital, Toronto, Canada

Abstract. Optical coherence tomography (OCT) is used to provide anatomical information of biological systems but can also provide functional information by characterizing the motion of intracellular structures. Dynamic light scattering OCT was performed on intact, control MCF-7 breast cancer cells and cells either treated with paclitaxel to induce apoptosis or deprived of nutrients to induce oncosis. Autocorrelations (ACs) of the temporal fluctuations of OCT intensity signals demonstrate a significant decrease in decorrelation time after 24 h in both the paclitaxel-treated and nutrient-deprived cell groups but no significant differences between the two groups. The acquired ACs were then used as input for the CONTIN deconvolution algorithm, and all produced CONTIN outputs with three distinct peaks for all experimental conditions. After 24 h of either paclitaxel treatment or nutrient deprivation, the area-under-the-curve (AUC) of the first peak increased significantly while the AUC of the third peak decreased significantly. These results lend strong support to the hypothesis that ACs acquired from cells are composed of multiple components that correspond to light scattered by different subcellular structures and organelles. [DOI: 10.1117/1.JBO.24.2.025002]

Keywords: cancer; dynamic light scattering; optical coherence tomography; CONTIN; deconvolution; speckle decorrelation.

Paper 180671R received Dec. 18, 2018; accepted for publication Feb. 1, 2019; published online Feb. 15, 2019.

1 Introduction

Speckle intensity in optical coherence tomography (OCT) is dependent on the size, spatial distribution, shape, and optical properties of scatterers within a resolution volume (RV).[1] In OCT imaging of living samples, temporal fluctuations in speckle intensity are observed due to scatterer motion,[2] which can include the flow of blood cells within vasculature, bulk movement of organs and tissues, and intracellular motion (IM). IM is the primary form of motion within *in vitro* cell samples that do not have vasculature, and it can be divided into two categories: passive and active motion. Passive motion refers to the random Brownian motion experienced by subcellular structures and organelles, and active motion refers to the deliberate motion within cells necessary to complete cellular functions, such as the transport of vesicles along microtubules and the morphological changes associated with mitosis and cytokinesis. The intensity fluctuations that arise from these movements can provide information about a biological system, such as the effectiveness of treatment on cancer cells.[3]

Dynamic light scattering (DLS) is a technique used to quantify the movement of particles by analyzing the autocorrelation (AC) function of light scattered by said particles.[4] Generally, an AC in DLS decays and the faster it decays, the greater the average rate of motion within the sample.[3] The integration of DLS techniques with OCT is referred to as dynamic light scattering optical coherence tomography (DLS-OCT) and was first proposed as a method to spatially localize IM during cell death. It has been demonstrated to have numerous biological applications, such as imaging cerebral blood flow,[5] observing extracellular matrix remodeling *in vitro*,[6] and measuring the growth of biofilms.[7] Lee et al.[8] developed a model to represent ACs from DLS-OCT that accounts for the finite size of voxels in OCT and the fact that multiple scatterers can exist within a voxel, each having a different rate of movement at any given time. Their model represents the overall AC from an RV as the superposition of individual ACs arising from each particle in the RV, each of which can experience one of three types of motion at any given time: static scatterers contribute to an unchanging DC value in the AC, flowing and diffusing scatterers contribute decaying terms, and particles moving in or out of the RV contribute to a delta function.

Previously, Farhat et al.[3] applied DLS-OCT to study changes in IM in acute myeloid leukemia cells between 0 and 48 h after treating the cells with cisplatin to induce apoptosis, a form of programmed cell death. To compare ACs at different time points, they defined a term known as the decorrelation time (DT) as the time for an AC to decay to half its maximum value. They observed that, 24 h after the start of treatment and persisting to 48 h, there was a significant decrease in DT, indicative of increased IM.[3] The increase in IM was likely caused by the morphological changes that occur in apoptotic cells, such as rounding and shrinking of the cell, dissolution of the organelles, and ultimately, the disintegration of the cell into smaller membrane-bound fragments known as apoptotic bodies.[9] However, an analysis based solely on the overall DT does not provide insight into the contributions of subcellular components to the measured signal.

In this work, we aim to use DLS-OCT to observe changes in the rate of IM in breast cancer cells that have either been treated with paclitaxel or deprived of nutrients and to gain insight into the contributions of subcellular scatterers to the OCT signal

*Address all correspondence to Michael C. Kolios, E-mail: mkolios@ryerson.ca

using a deconvolution algorithm commonly used in DLS. We hypothesize that the DTs acquired from paclitaxel-treated cells will decrease after 24 h since paclitaxel is known to induce apoptosis in breast cancer cells[10] and apoptosis is characterized by vigorous IM. Moreover, the structural changes associated with apoptosis are consistent across different cell types.[9] However, cells require energy in the form of ATP to undergo apoptosis,[11] and cells that are deprived of nutrients are rapidly depleted of ATP. Instead of apoptosis, nutrient-deprived cells are more likely to experience oncosis, which is a form of ischemic or accidental cell death. Oncosis is characterized by predictable changes in cellular morphology, including swelling of the cell and rupture of the plasma membrane, ultimately causing intracellular components to escape from the cell.[9] We hypothesize that the DTs acquired from nutrient-deprived cells will also decrease due to increased passive IM.

Particles experiencing diffusive motion, such as the byproducts of apoptosis and oncosis, contribute to the DLS-OCT ACs.[8] Deconvolution algorithms can be used to decompose an AC into component exponential decay functions, which is an ill-posed problem as there can exist more than one mathematical solution for a given AC. CONTIN is a deconvolution algorithm commonly used in DLS to determine the distribution of exponential decay functions from polydisperse solutions containing particles with different sizes and rates of diffusion.[12] To overcome the ill-posed nature of AC deconvolution and produce repeatable and accurate outputs, CONTIN utilizes constraints on the relaxation time distributions; this renders the algorithm less robust as it requires prior knowledge (such as the range of scatterer sizes) and cannot characterize an unknown system in a reliable manner.[12] The CONTIN output is a relaxation time distribution that depicts the contribution of various exponential decay functions to the overall AC as a function of decay time. The peaks in the CONTIN output describe the contributions of populations of light scatterers with similar sizes or diffusion rates to the overall AC. The intracellular environment represents a polydisperse and heterogeneous solution, and we hypothesize that when using ACs acquired from DLS-OCT imaging of breast cancer cells as input into the CONTIN algorithm, the distributions will have multiple peaks that arise from the light scattered by various subcellular structures, such as cellular nuclei and mitochondria.

2 Methods

2.1 *Biological Sample Preparation*

Cell samples were prepared from breast ductal carcinoma cells (MCF-7). For each experimental trial, $\sim 2 \times 10^7$ cells were grown in a 37°C incubator in a 75-cm^2 cell culture flask containing 10 mL of Dulbecco's modified Eagle medium (DMEM) containing 4.5 g/L of glucose, and supplemented with 1% streptomycin and penicillin, 10% fetal bovine serum, and 1% insulin. The cells were separated evenly into three 75-cm^2 cell culture flasks 24 h prior to the start of any treatments, with each flask containing $\sim 7 \times 10^6$ cells and the same concentration of media and supplements as the initial flask but without insulin as it inhibits MCF-7 sensitivity to paclitaxel.[13]

The three samples were left in the 37°C incubator for 24 h to allow the cells to completely adhere to the bottom surface of the flasks. After this time, two of the flasks were treated with 20 ng/mL paclitaxel. The cells from the untreated sample were made into a pellet and imaged at three different times: immediately after pellet formation, and then 24 and 48 h after pellet formation. Between each time point, a small amount of phosphate-buffered saline (PBS) was added to the untreated cell pellet to keep the cells from drying out, and the pellet was stored at 37°C. The two samples that had been treated with paclitaxel were imaged at one time point each, after 24 and 48 h of paclitaxel exposure, respectively, and then immediately discarded.

To form a pellet for imaging, all media was carefully removed from a cell sample, which was then washed with 1× PBS. About 0.25% trypsin and ethylenediaminetetraacetic acid were then applied to the sample for 5 min to suspend cells that adhered to the surface of the flask and/or to each other. The suspended cells were then placed into a small pellet container and centrifuged at 500 g for 10 min to form a tightly packed cylindrical pellet with a diameter of 8 mm and a height of ~0.6 to 0.8 mm.

2.2 *Optical Coherence Tomography Data Acquisition*

OCT imaging was performed using a Thorlabs Inc. (Newton, New Jersey) swept-source OCT system with a central wavelength of 1310 nm, a bandwidth of 100 nm, and lateral and axial resolutions of ~25 and 12 μm, respectively. Each time a sample was imaged, 500 consecutive two-dimensional frames were recorded at a frame rate of 333 Hz, with each image spanning ~1 mm in the transverse direction. Pixels in the images were ~10 μm × 10 μm in size. From each set of frames, a region of interest (ROI) measuring 100 pixels in the transverse direction and 3 pixels in the axial direction was selected, starting ~30 μm below the top surface of the cell pellet to avoid partial volume effects. A sample *b*-mode OCT image and ROI selection are shown in Fig. 1. For each pixel in the ROI, the intensity was plotted as a function of time across all frames, and the AC was calculated by taking the inverse Fourier transform of the power spectrum of the intensity signal. The ACs from all 300 pixels were then averaged, and the static component was subtracted from the average AC to remove the contribution from static scatterers. The average AC from the ROI was then normalized to have a maximum value of 1. To account for heterogeneity in the cell pellets, each sample was imaged 10 times at different spatial locations.

2.3 *Autocorrelation Analysis*

The mean ACs decayed to 50% of their maximum value within two 3-ms time steps, so the DT was not defined as the time for an AC to decay to half its maximum value, as was done by Farhat et al.[3] Instead, all ACs were fitted to exponential decay curves, and the DT for each AC was defined as the relaxation time of the best-fit exponential decay curve.

Each measured AC was used as an input into the CONTIN algorithm. We constrained the relaxation time distribution to be within the range of 0.1 to 1000 ms. The upper limit of the range was chosen to be >750 ms, which was the total length of each AC, while the lower limit of the range was set to be significantly less than the temporal resolution of our OCT system, which was 3 ms. The regularization parameter was initially set to 0 for a pilot run, but the resulting relaxation time distribution was noisy. The regularizer was then increased to 0.1 in a subsequent trial run. The number of peaks and location of the peaks in the distributions did not change when the regularizer was increased, but the noise in the distributions was reduced significantly at

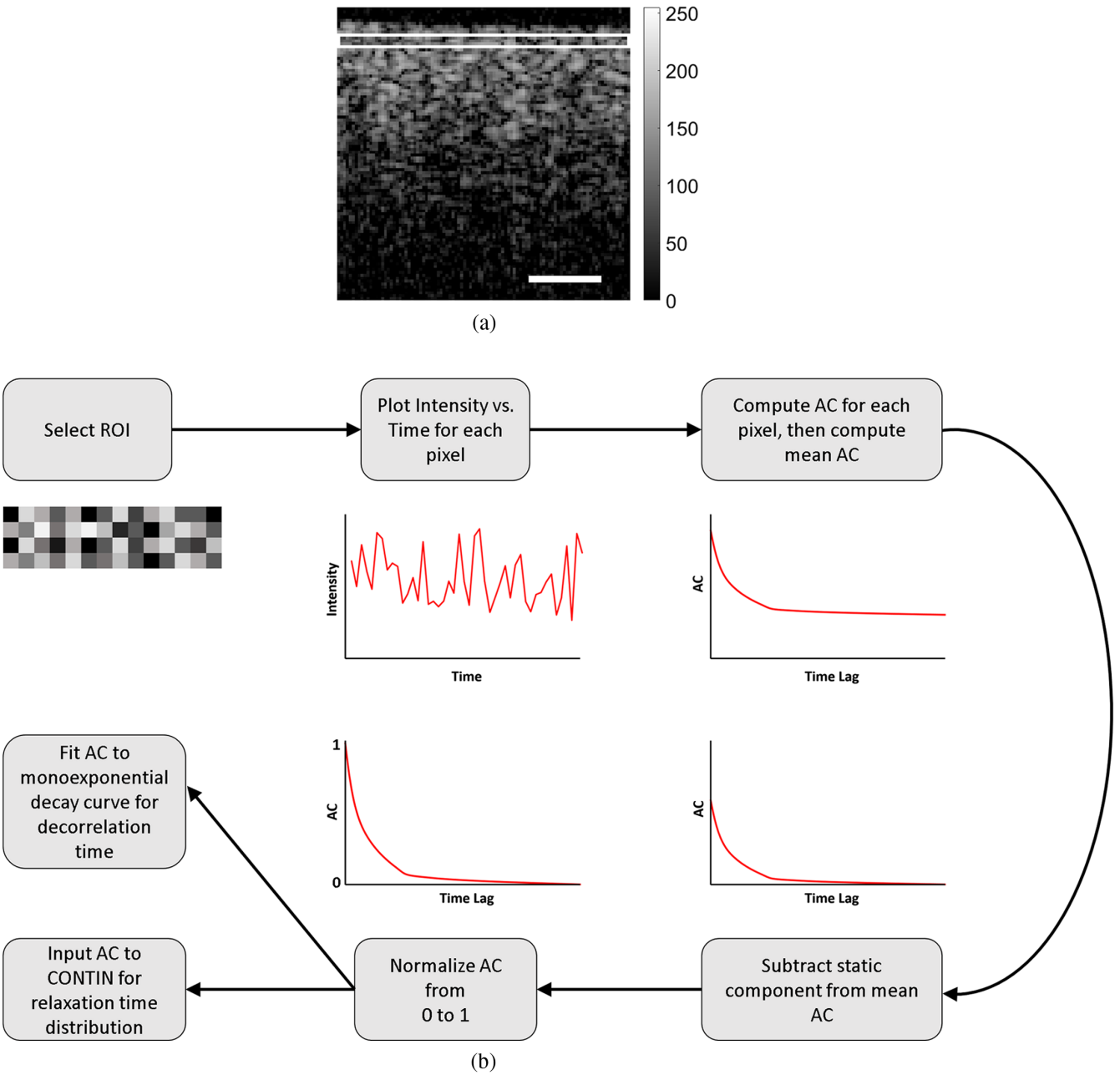

Fig. 1 (a) OCT *b*-mode image of an MCF-7 cell pellet. The ROI is indicated by the white rectangle. The color bar indicates pixel image intensity between 0 and 255. The scale bar represents 0.25 mm. (b) Diagram depicting the postprocessing pipeline used in this study to acquire DT and relaxation time distribution from an ROI.

the expense of slightly wider peaks so the regularizer was chosen to be 0.1 for all AC deconvolution analysis.

2.4 *Validation of Treatment Effectiveness*

To confirm that the paclitaxel and nutrient-deprivation treatments had an effect on the cells, $\sim 3 \times 10^6$ cells from one of the experimental trials were evenly divided into three 25-cm^2 cell culture flasks, each containing 5 mL of DMEM containing 4.5 g/L of glucose and supplemented with 1% streptomycin and penicillin and 10% fetal bovine serum. The cells were then incubated at 37°C for 24 h to allow the cells to adhere to the bottom surface of the flasks. After this time, the confluence in all three flasks was close to 100%. About 20 ng/mL paclitaxel was added to one of the flasks, the media in another flask was replaced with 1× PBS, and the third flask was used as a control group. All three flasks were imaged with a standard light microscope, and then again after 24 and 48 h to observe differences in the cells over time after exposure to treatment.

3 Results and Discussion

The light microscopy images (Fig. 2) obtained from MCF-7 cell samples showed significant changes in cellular morphology in the paclitaxel-treated and nutrient-deprived groups but not in the control group. After 24 h of paclitaxel exposure, sample

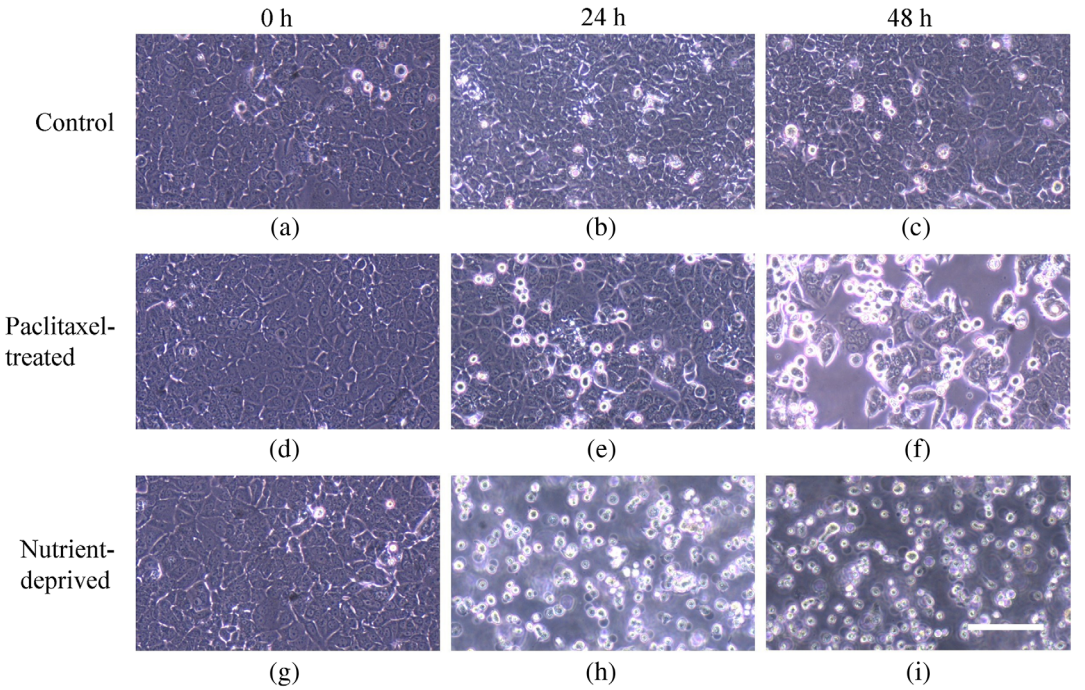

Fig. 2 Bright-field microscopy images of control cells at (a) 0 h, (b) 24 h, and (c) 48 h; paclitaxel-treated cells at (d) 0 h (pretreatment), (e) 24 h, and (f) 48 h; nutrient-deprived cells at (g) 0 h (pretreatment), (h) 24 h, and (i) 48 h. The scale bar represents 0.2 mm.

confluence was reduced, and many suspended cells were observed in the flask, which indicates loss of adherence and which is a characteristic change that occurs during cell death.[14] Cells with irregular shapes were also observed, likely indicative of membrane blebbing. After 48 h of paclitaxel exposure, cell adherence was further reduced, and more irregularly shaped cells were observed. In the nutrient-deprivation cell group, adherence of the cells to the flask bottom was reduced to 0% after 24 h. In contrast, there was no loss of confluence in the control group after 24 or 48 h, and a very small number of nonadherent cells were observed. Though these images do not directly confirm the presence of cell death or differentiate between different modes of cell death, they indicate a significant treatment response in both the paclitaxel-treated and nutrient-deprived cell groups.

ACs obtained from nutrient-deprived and paclitaxel-treated cell samples are shown in Fig. 3. A significant drop is observed in each of the ACs within the first 6 ms, which can be attributed to scatterers moving in and out of RVs within the ROI. The curves for the nutrient-deprived and paclitaxel-treated samples decayed more rapidly than the curves for the untreated cell samples, which indicates greater motion in the treated samples.[3]

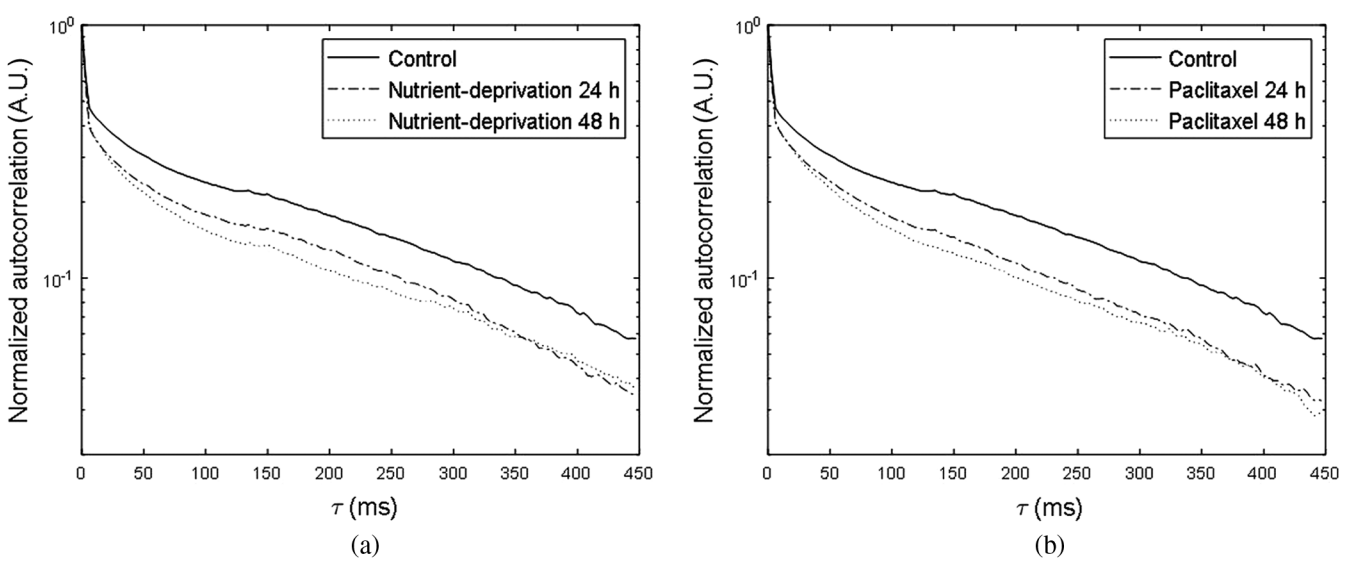

Fig. 3 ACs obtained from MCF-7 cell pellets (a) control and treated with 20 ng/mL paclitaxel and (b) control and deprived of nutrients and growth factor. Each curve represents the average of 10 measurements from within each sample.

All experiments were performed in triplicate, on different weeks and using different cell passages, and demonstrated good technique repeatability despite biological variations and inherent heterogeneity between samples.

The DTs computed by fitting exponential decay curves to the mean ACs are plotted as a function of treatment duration in Fig. 4 to provide a quantitative assessment of the change in AC decay as a function of treatment time. In all experimental trials, a statistically significant drop in the DT ($p < 0.01$) was observed after either 24 or 48 h of paclitaxel exposure or nutrient-deprivation when compared to the untreated cell samples. However, there was no statistically significant difference ($p > 0.05$) between the DTs from any of the treated groups, suggesting that the technique could not distinguish between the treatment types and durations used in these trials with the approach presented. We hypothesize that both paclitaxel-treatment and nutrient-deprivation lead to an increase in IM due to structural changes that occur within the cells, and that many of these changes occur within the first 24 h of treatment with a diminishing effect within the next 24 h. Many active processes that occur during apoptosis can lead to a net increase in the average rate of IM, including cytoskeletal restructuring and nuclear and cellular fragmentation.[9] Passive motion of intracellular components or cell fragments can increase after apoptosis as well, as the process reduces cells to fragmented bodies that are smaller and can have greater diffusion compared to organelles in intact cells. Oncosis results in cellular swelling and rupture that could reduce steric hindrance and allow for organelles and particles to diffuse more freely.[9]

A representative CONTIN output from one of the ACs acquired from MCF-7 cells is shown in Fig. 5. A total of 150 ACs were used as input into CONTIN (30 each from untreated cells, and 24- and 48-h paclitaxel-treated and nutrient-deprived cells) and each produced an output with three distinct peaks, which suggests that the ACs can be decomposed into three main components. The mean central DTs of the peaks were 2.5 ± 0.1 ms, 17.2 ± 4.8 ms, and 223.6 ± 23.5 ms. There was no statistically significant difference ($p > 0.05$) between the mean central DTs of the peaks between untreated samples and those that had undergone various treatments.

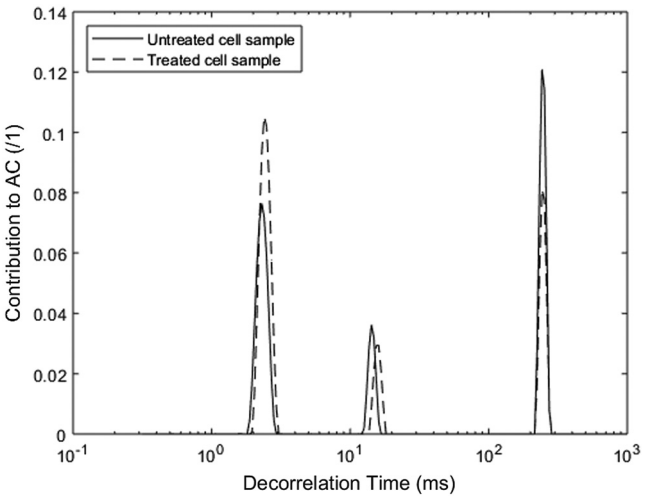

Fig. 5 Sample CONTIN outputs depicting the contribution of various exponential decay functions to the AC as a function of their DTs. The solid line depicts a representative sample CONTIN output from an untreated cell sample while the dashed line depicts a representative sample CONTIN output from 48-h nutrient-deprived cells.

To compare the CONTIN outputs from the different samples, we computed the area-under-the-curve (AUC) of each of the peaks for all CONTIN output distributions. For simplicity, the peaks are referred to as P1, P2, and P3 in order of ascending mean central DT. The AUCs of the three peaks as a function of treatment type and duration are shown in Fig. 6. In both the nutrient-deprived and paclitaxel-treated samples, a statistically significant increase ($p < 0.05$) was observed in the AUC of P1 and a statistically significant decrease ($p < 0.02$) was observed in the AUC of P3 after 24 or 48 h of treatment compared to the control group. No statistically significant differences ($p > 0.05$)

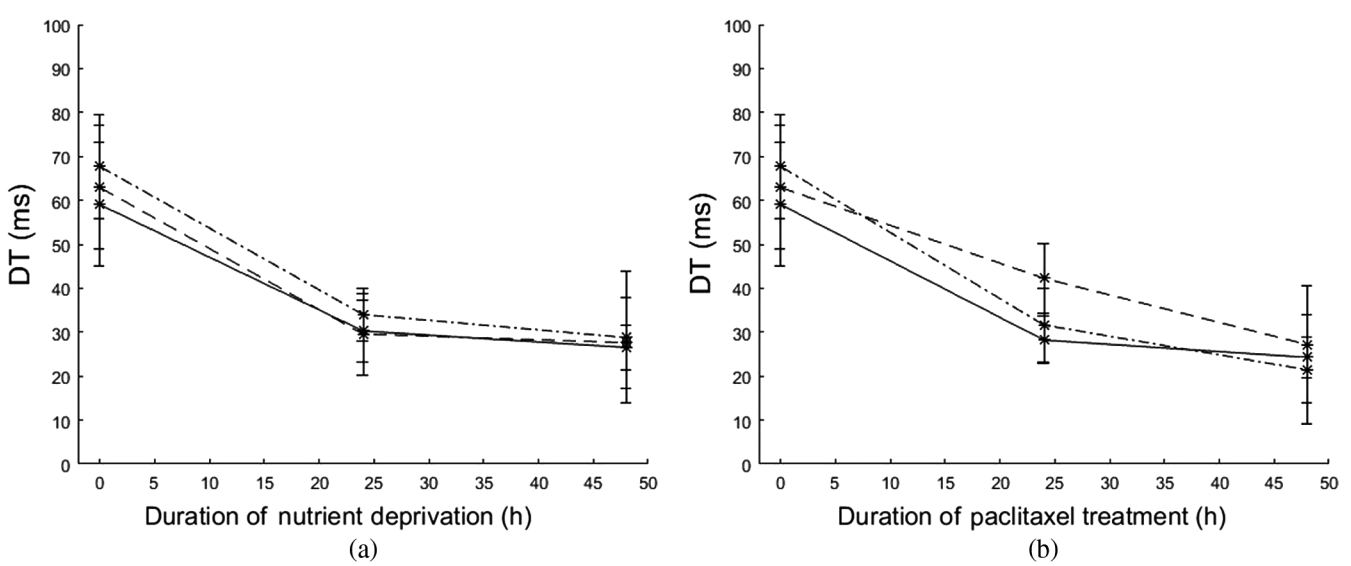

Fig. 4 DTs obtained from MCF-7 cell pellets (a) deprived of nutrients and growth factors and (b) treated with 20 ng/mL paclitaxel, as a function of treatment duration. The 0-h measurements were taken prior to treatment and represent a control DT. Each line represents a separate experiment (three in total). Error bars represent the standard deviation across 10 separate measurements at different locations from within each sample.

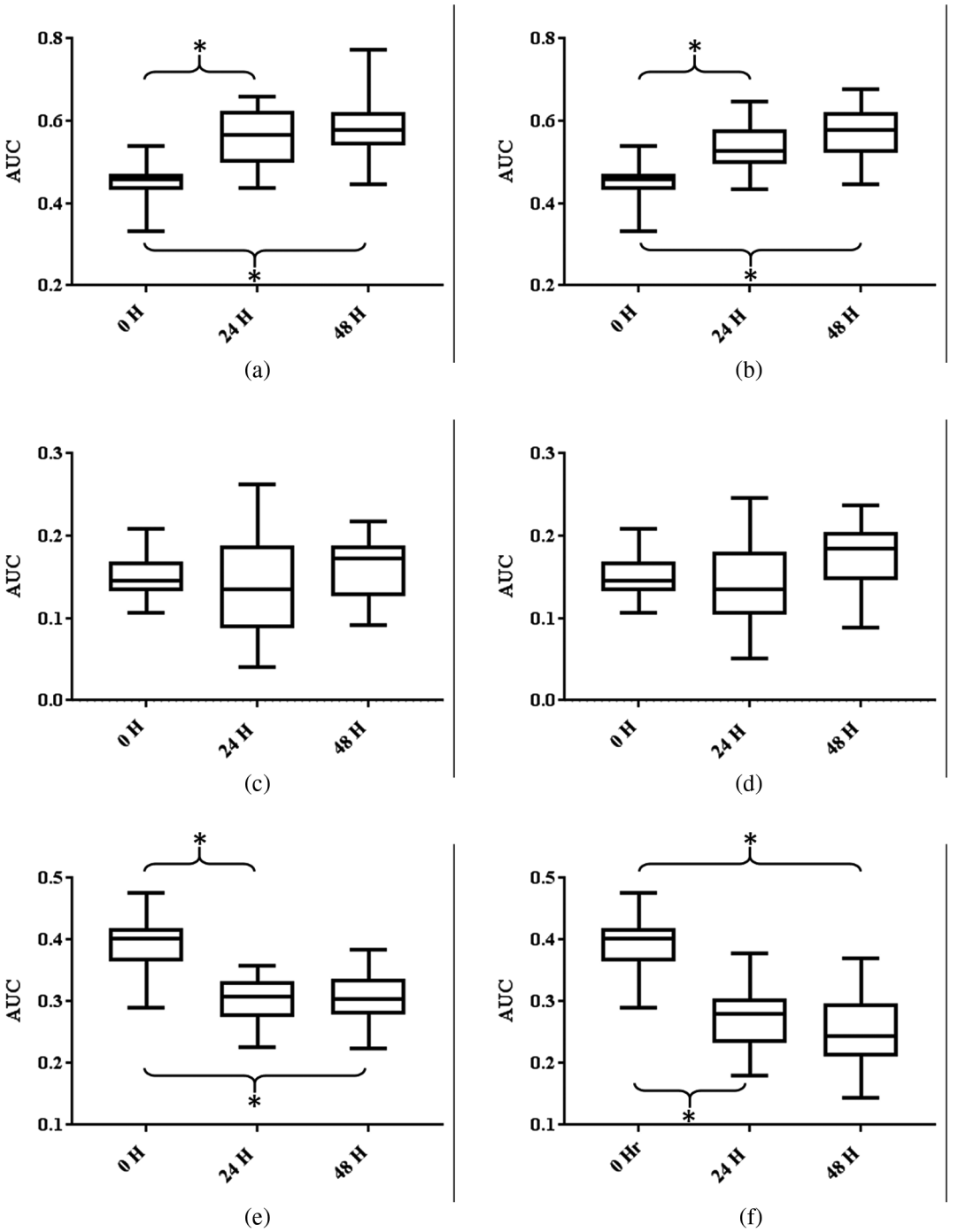

Fig. 6 AUC of P1 in (a) nutrient-deprived cells and (b) paclitaxel-treated cells as a function of treatment. AUC of P2 in (c) nutrient-deprived cells and (d) paclitaxel-treated cells as a function of treatment. AUC of P3 in (e) nutrient-deprived cells and (f) paclitaxel-treated cells as a function of treatment. Box plot whiskers show the minimum and maximum values in each group. The central line within the box plots is the group median. The top and bottom limits of the boxes are the 75th and 25th percentiles, respectively. Each box represents a group of 30 measurements. No outliers were detected. $^{*}p \ll 0.01$.

were observed in the AUC of P2 between any groups, or in the AUCs of P1 and P3 between any of the treated groups.

The values generated using the ACs as input into the CONTIN algorithm can be used to differentiate between the treated and untreated cells based on changes in the AUCs of P1 and P3. Experiments demonstrated good technique repeatability. Though fitting a single exponential decay curve to each AC was sufficient for differentiating the ACs and correlating these to treatment response, we believe that the values produced using the CONTIN algorithm may provide more detailed information about scattering structures in the cells studied. We speculate that each of the three peaks in the CONTIN output distributions arose from light scattered by different intracellular components. Since P1 had a central DT of 2.5 ± 0.1 ms, which is smaller than the temporal resolution of our system (3 ms), we suspect that these results related to P1 may have

primarily arisen from a combination of light backscattered by very small structures, such as lysosomes and vesicles, which would have rapid diffusive motion. Small particles of this size range are expected to move in and out of the RV for the timescales measured. Other significant scattering structures within cells include mitochondria[15] and nuclei,[16] and we suspect that they may have been the dominant scattering structures that contributed to P2 and P3, respectively. We speculate that the increase in the AUC for P1 that occurs after both treatments is caused by the breakdown of larger structures into smaller structures, and an increase in the motion in and out of each RV. Furthermore, we speculate that the decrease in the AUC of P3 may have arisen from the breakdown of nuclei, resulting in such structures scattering less light and therefore contributing less to the AC.

4 Conclusions

We have shown through this work that DLS-OCT techniques can be used to differentiate between untreated and treated MCF-7 breast cancer cells 24 h after the start of treatment for two different types of treatments, with good repeatability. However, our techniques could not distinguish between the different types of cell death at the 24- or 48-h timepoints using this approach. Further investigation of the ACs within the first 24 h of treatment to test for differences between the chemotherapy-treated and nutrient-deprived groups, with better temporal resolution to determine greater differences in changes in the ACs, is the subject of future work.

This work presents the first time the CONTIN deconvolution algorithm was used to characterize ACs from *in vitro* cell samples as superpositions of multiple exponential decay functions. The results were reproducible across three separate trials, evidencing the effectiveness of the technique for the study of MCF-7 cell pellets. However, it should be noted that cell pellets are rather simple systems compared to *in vivo* models because they are relatively motionless on an extracellular level. In living animals or humans, the presence of bulk motion, blood flow, respiration, or other types of movement could affect the fluctuating OCT signal; these additional sources of movement could contaminate the ACs with noise or artifacts that could render CONTIN less effective. We anticipate that corrections would have to be performed on DLS data acquired *in vivo* to account for these additional factors.

Future work should aim to concurrently perform DLS-OCT while also quantifying the motion of light-scattering organelles, such as nuclei and mitochondria, using methods such as confocal microscopy. This may provide a better understanding of the relationship between the IM of specific intracellular targets and the AC decay. Furthermore, investigation into the motion of individual scatterers may provide insights related to the origin of the three peaks observed in the CONTIN output distributions and what intracellular structures contribute to these peaks.

Disclosures

The authors have no relevant financial interests and no potential conflicts of interest to disclose.

Acknowledgments

This work was funded by the Natural Sciences and Engineering Research Council of Canada (No. 216986-2012) and Ryerson University. Funding to purchase the equipment was provided by the Canada Foundation for Innovation, the Ontario Ministry of Research and Innovation, and Ryerson University. The authors would also like to acknowledge Elizabeth Berndl for her assistance and expertise with the experiments and Kirsten Cardinell for her aid in figure design.

References

1. J. Schmitt, S. Xiang, and K. Yung, "Speckle in optical coherence tomography," *J. Biomed. Opt.*, **4**(1), 95 (1999).
2. A. Mariampillai et al., "Speckle variance detection of microvasculature using swept-source optical coherence tomography," *Opt. Lett.* **33**(13), 1530–1532 (2008).
3. G. Farhat et al., "Detecting apoptosis using dynamic light scattering with optical coherence tomography," *J. Biomed. Opt.* **16**(7), 070505 (2011).
4. N. A. Clark, J. H. Lunacek, and G. B. Benedek, "A study of Brownian motion using light scattering," *Am. J. Phys.* **38**(5), 575–585 (1970).
5. J. Lee et al., "Quantitative imaging of cerebral blood flow velocity and intracellular motility using dynamic light scattering-optical coherence tomography," *J. Cereb. Blood Flow Metab.* **33**(6), 819–825 (2013).
6. R. Blackmon et al., "Imaging extracellular matrix remodeling in vitro by diffusion-sensitive optical coherence tomography," *Biophys. J.* **110**(8), 1858–1868 (2016).
7. N. Weiss et al., "Measurement of biofilm growth and local hydrodynamics using optical coherence tomography," *Biomed. Opt. Express* **7**(9), 3508–3518 (2016).
8. J. Lee et al., "Dynamic light scattering optical coherence tomography," *Opt. Express* **20**(20), 22262 (2012).
9. G. Majno and I. Joris, "Apoptosis, oncosis, and necrosis. An overview of cell death," *Am. J. Pathol.* **146**(1), 3–15 (1995).
10. D. Saunders et al., "Paclitaxel-induced apoptosis in MCF-7 breast-cancer cells," *Int. J. Cancer* **70**, 214-220 (1997).
11. G. E. Kass et al., "Chromatin condensation during apoptosis requires ATP," *Biochem. J.* **318**(3), 749–752 (1996).
12. A. Scotti et al., "The CONTIN algorithm and its application to determine the size distribution of microgel suspensions," *J. Chem. Phys.* **142**(23), 234905 (2015).
13. A. Miglietta et al., "Insulin can modulate MCF-7 cell response to paclitaxel," *Cancer Lett.* **209**(2), 139–145 (2004).
14. S. Magali and H. Steller, "Letting go: modification of cell adhesion during apoptosis," *J. Biol.* **8**(5), 49 (2009).
15. R. Pasternack, J. Zheng, and N. Boustany, "Optical scatter changes at the onset of apoptosis are spatially associated with mitochondria," *J. Biomed. Opt.* **15**(4), 040504 (2010).
16. J. Mourant et al., "Light scattering from cells: the contribution of the nucleus and the effects of proliferative status," *J. Biomed. Opt.* **5**(2), 131–137 (2000).

Nico J. J. Arezza is a PhD student at the University of Western Ontario. He received his BEng degree in biomedical engineering and MSc degree in biomedical physics from Ryerson University in 2016 and 2018, respectively. His current research interests include diffusion magnetic resonance imaging and neurological disorders. He is a member of SPIE and the International Society for Magnetic Resonance in Medicine.

Marjan Razani is a postdoctoral fellow at Ryerson University. She received her PhD in biomedical physics from Ryerson University in 2016. Her research focuses on applications of optical coherence tomography.

Michael C. Kolios is a professor in the Department of Physics and an associate dean of research and graduate studies in the Faculty of Science, Ryerson University. His work focuses on the use of ultrasound and optics in the biomedical sciences.